Winter interactions between aerosols and weather regimes in the North-Atlantic European region

Ménégoz Martin, Virginie Guemas, David Salas y Melia, Voldoire Aurore

JOURNAL OF GEOPHYSICAL RESEARCH, VOL. 115, D09201, doi:10.1029/2009JD012480, 2010

Winter interactions between aerosols and weather regimes in the North Atlantic European region

M. Ménégoz,[1] V. Guemas,[1,2] D. Salas y Melia,[1] and A. Voldoire[1]

Received 14 May 2009; revised 4 December 2009; accepted 21 December 2009; published 4 May 2010.

[1] This study aims at understanding the winter interactions between aerosols and weather regimes in the North Atlantic European region. As a first step, a 6 year simulation of sulfate, black carbon (BC), and dust is performed with a Chemical Transport Model (CTM), forced by the meteorological data issued from the European Centre for Medium-range Weather Forecast Integrated Forecast System model. The CTM uses the emissions inventory of aerosols and precursor gases provided by the AERosol Comparison between Observations and Models project. In this experiment, atmospheric dynamical processes associated with the different regimes can impact by up to 25% the burden of sulfate and BC and by up to 80% the burden of mineral dust, through the modification of deposition, transport, and chemistry processes. As a second step, the patterns of aerosol anomalies induced by each weather regime are used to force experiments performed with an Atmosphere General Circulation Model. The mean persistence of the negative phase of the North Atlantic Oscillation (NAO–) and the zonal regime is reduced by 1.78 and 0.88 days, respectively, when the atmosphere is forced with the patterns of aerosols induced by the zonal regime and the blocking regime, respectively. This suggests that the interaction between the atmosphere and its aerosol concentration could destabilize the NAO– regime that occurs after a zonal episode. The same conclusion can be set out for a zonal regime that occurs after a blocking episode.

Citation: Ménégoz, M., V. Guemas, D. Salas y Melia, and A. Voldoire (2010), Winter interactions between aerosols and weather regimes in the North Atlantic European region, *J. Geophys. Res.*, *115*, D09201, doi:10.1029/2009JD012480.

1. Introduction

[2] Atmospheric aerosols are known to influence substantially the radiation budget of the Earth through scattering and absorption (direct radiative forcing [e.g., *Ångström*, 1962; *McCormick and Ludwig*, 1967; *Schulz et al.*, 2006]) as well as through clouds, because of their role as condensation nuclei (indirect radiative forcing [e.g., *Twomey*, 1977; *Albrecht*, 1989; *Lohmann and Feichter*, 2005]). The combination of these effects and its feedback is up to now quite uncertain [*IPCC*, 2007], because of the complexity of the physical and chemical properties of the aerosol components. However, the atmospheric concentration of aerosols and the aerosol radiative forcing could be estimated thanks to global simulations, such as those realized, for example, in the context of the AEROsol Comparison between Observations and Models (AEROCOM) project [*Textor et al.*, 2006; *Schulz et al.*, 2006]. The total global aerosol radiative forcing is estimated to be negative, evaluated to -1.2 W m^{-2} (range, -2.7 to -0.4 W m^{-2}) [*IPCC*, 2007]. Over Europe, it has been shown that the aerosol radiative forcing is strongly dependent on the aerosol distribution, which can vary significantly both seasonally and from one year to another [*Hohenegger and Vidale*, 2005; *Marmer et al.*, 2007]. Aerosol radiative forcing is expected to have an impact on the variability of the atmospheric circulation over the North Atlantic European (NAE) region and, as a result, to imply changes in surface temperature, precipitation, and storminess that affect Europe. The goal of the present study is to assess the interaction between wintertime atmospheric variability and aerosol distributions. For this purpose, we use the decomposition of the atmospheric state into weather regimes [*Vautard*, 1990].

[3] These weather regimes can be viewed as the preferred states of the atmospheric circulation. Each of them has a mean persistence of about 1 week. The recent study by *Cassou* [2008], using this concept of weather regimes, suggests a potential predictability of the atmospheric circulation more than 1 week in advance in the NAE region. A better understanding of the mechanisms favoring the occurrence of each winter weather regime is therefore essential to improve their predictability and the predictability of associated patterns of temperature, precipitation, and storminess. It is well known that the variability of the atmospheric circulation is primarily driven by internal dynamical processes. However, some external forcing can modulate the temporal evolution of the atmospheric state, e.g., the sea surface temperature variability [*Cassou et al.*, 2004]. Here we investigate the interactions between aero-

[1]CNRM/GAME, Météo-France, Toulouse, France.
[2]LSCE, UMR1572, IPSL, UVSQ, CNRS, Gif-sur-Yvette, France.

0148-0227/10/2009JD012480

sols and weather regime over the NAE region. This topic has received very little attention up to now.

[4] It is complex to model the interactions between the atmospheric aerosol concentration and the weather pattern, because aerosol concentration can be strongly modified by meteorological conditions, and in return the weather pattern may be affected by the presence of aerosols in the atmosphere. Most of the aerosol-climate interaction studies use climate models embedding aerosol modules in Atmosphere General Circulation Models (AGCMs) [e.g., *Kirkevag et al.*, 2008; *Reddy et al.*, 2005; *Koch*, 2001]. This approach (referred to as "online") is quite interesting, because all the retroactions between aerosols and climate are taken into account in the simulations. Other studies are based on AGCM simulations using aerosol climatologies produced separately by a Chemical Transport Model (CTM) approach (referred to as "offline" [e.g., *Pitari et al.*, 2002; *Rongming et al.*, 2001]). In such an approach, the aerosol simulation realized with the CTM is generally performed with accurate meteorological analyses of an operational model, which allows us to simulate quite realistically the atmospheric concentration of aerosol.

[5] In our study, we used an off-line simulation to obtain an accurate description of the aerosol burden associated with each weather regime. For this purpose, we used the Modèle de Chimie Atmosphérique de Grande Echelle (MOCAGE) CTM to simulate the distribution of sulfate, black carbon (BC), and desert dust from 2000 to 2005. MOCAGE is forced with the meteorological analyses from the European Centre for Medium-range Weather Forecast Integrated Forecast System (ECMWF IFS) model. Based on this simulation, a data set of daily aerosol burdens was created. The distribution of the burden, sinks, and sources of each aerosol species is evaluated for each weather regime. This is the first step of our study. In the second step, the different patterns of aerosol anomalies induced by the different weather regimes are used to drive several simulations off-line, made with the Action de Recherche Petite Échelle Grande Échelle (ARPEGE-Climat) AGCM. In these atmospheric simulations, we investigated, in particular, the role of the aerosol burden on the persistence of weather regimes or their transition toward another weather regime during winter. The CTM used and the aerosol simulation are presented in section 2. The impact of North Atlantic weather regimes on the aerosol distributions is analyzed in section 3. Section 4 presents the AGCM and investigates the feedback of the aerosol distributions on persistence of the north Atlantic weather regime. Conclusions are drawn in section 5.

2. Aerosol Simulation

[6] For this study, an aerosol simulation was performed with the MOCAGE global CTM [*Teyssèdre et al.*, 2007] (CNRM/GAME/Météo-France). MOCAGE has been designed for a range of applications, from regional air quality studies to global climate studies dealing with the evolution of tropospheric and stratospheric chemical species. The version used in this study was adapted to represent trace gases and aerosols at the global scale and is briefly presented in section 2.1; it is described in detail by *Ménégoz et al.* [2009].

2.1. General Features of the CTM

[7] In our simulation, MOCAGE is used on a T42 Gaussian grid (about 2.8° × 2.8° horizontal resolution) and with 47 vertical sigma pressure layers from the surface to 5 hPa. Seven levels are within the planetary boundary layer, 20 in the free troposphere, and 20 in the stratosphere. The first layer is ~40 m thick, while the resolution above 300 hPa is constant with altitude, around 800 m. A semi-Lagrangian scheme is used for the advection of tracers and chemical compounds. Based on the work of *Williamson and Rasch* [1989], it is described in detail by *Josse et al.* [2004]. Time steps are 1 h for advection and 15 min for subgrid-scale processes. The turbulent diffusion follows *Louis* [1979], whereas the convection scheme (mass-flux-type) is that of *Bechtold et al.* [2001]. The representation of dry deposition for gases, based on the work of *Wesely* [1989], was presented by *Michou and Peuch* [2002]. In-cloud and below-cloud scavenging representation for gases was presented by *Teyssèdre et al.* [2007].

2.2. Aerosol Representation in the Model

[8] MOCAGE can simulate the evolution of three types of aerosols: sulfate, BC, and dust. Organic carbon (OC) and sea-salt aerosols are not yet implemented in the model. BC and dust are emitted directly into the atmosphere, whereas sulfate is produced by chemical reactions involving precursor gases. Some of these gases are natural (dimethylsulfide [DMS] emitted by the ocean), and others are anthropogenic (SO_2 and H_2S). Concentrations of the oxidant (OH, H_2O_2, O_3, and NO_3) are prescribed and provided by a 1 year MOCAGE simulation with the full chemical scheme described by *Teyssèdre et al.* [2007]. Representation of the sulfur cycle, based on the study by *Pham et al.* [1995], was described by *Ménégoz et al.* [2009]. Both aqueous and gaseous phase reactions produce sulfate. The parameterization of the dry deposition was based on the work of *Seinfeld and Pandis* [2006]; its implementation in MOCAGE was presented by *Nho-Kim et al.* [2004]. The sedimentation velocity, negligible for BC and sulfate aerosols, is essential for the representation of large dust aerosols. Its parameterization was adapted from Stokes law [*Seinfeld and Pandis*, 2006]. Below-cloud scavenging depends on the collision efficiency between aerosols and cloud droplets, as computed by *Seinfeld and Pandis* [2006]. In-cloud scavenging is simulated according to the scheme of *Langner and Rodhe* [1991]. BC and sulfate transfer efficiencies from solid to aqueous phase are adjusted from the observations of *Kasper-Giebl* [2000], as presented by *Ménégoz et al.* [2009]. This parameter is considered to be identical for mineral dust and BC. For each type of aerosol, the total distribution can be represented by several modes, all of which have a lognormal distribution. Diameter, standard deviation, and fraction number of the different modes for each aerosol are presented in Table 1. Distributions are discretized into bins of different sizes in MOCAGE, as described by *Martet et al.* [2009]. The last column of Table 1 shows the different bins used for each aerosol. In MOCAGE simulations, the chemical production of sulfate and the direct emissions of BC and mineral dust are injected into the atmosphere according to the distribution shown in this Table 1.

Table 1. Diameters, Standard Deviation, and Number Fraction of Lognormal Distribution for Mineral Dust, Black Carbon, and Sulfate

Aerosol	Distribution[a]			Numbers and Sizes of Bins Used in the Model[b] (m)
	Diameter (μm)	Standard Deviation	Number Fraction	
Mineral dust modes	0.22	1.59	0.38	5 bins
	0.63	2.0	0.62	(1.00E-8 to 6.31E-8; 6.31E-8 to 3.98E-7; 3.98E-7 to 2.51E-6; 2.51E-6 to 1.58E-5; 1.58E-5 to 1.00E-4)
Black carbon modes	0.015	1.8	0.92	4 bins
	0.040	1.8	0.08	(1E-9 to 1E-8; 1E-8 to 1E-7; 1E-7 to 1E-6; 1E-6 to 1E-5)
Sulfate modes	0.015	1.8	0.98331	4 bins
	0.04	1.8	0.01650	(1E-9 to 1E-8/1E-8 to 1E-7/1E-7 to 1E-6/1E-6 to 1E-5)
	0.5	2	0.00019	

[a]Based on AEROCOM indications.
[b]Distribution in bin size used in the MOCAGE model.

2.3. The 2000–2005 Simulation

[9] A simulation of the years 2000–2005 was computed for the aim of this study. In this simulation, air temperature, humidity, pressure, and wind components used to drive MOCAGE were provided from 6 h analyses obtained by the ECMWF IFS model. For the 6 years of the simulation, we used the AEROCOM global emissions inventory representative of the year 2000 [*Dentener et al.*, 2006]. This inventory is one of the commonly used inventories of aerosols and precursor gases to perform aerosol simulations. Emissions of SO_2, H_2S, SO_4^{2-}, and BC are constant over the year, except for biomass burning emissions, which have monthly variations. The AEROCOM inventory considers daily variations of DMS and dust emissions. However, we used monthly averages for these fields because we assume that daily variations of these emissions are very different from one year to another, and it would not make sense to take them into account in a 6 year simulation. We assumed that 2.5% of the anthropogenic elementary sulfur is directly emitted as SO_4^{2-}, the rest being SO_2.

2.4. Validation of the Simulation

[10] Before studying our aerosols simulation over the NAE region, it is necessary to evaluate the ability of the model to describe the main sources and sinks for each type of aerosol. Table 2 shows global aerosol burdens, sinks, and sources computed in 2000 by MOCAGE and the multimodel mean from the AEROCOM intercomparison exercise. Aerosol burdens simulated by MOCAGE are in the range of the burdens simulated by AEROCOM models. The MOCAGE BC burden is equal to the mean of that in the AEROCOM models. Concerning this aerosol, dry deposition is more efficient in MOCAGE than in all other models, but it is compensated by wet deposition, which is lower in MOCAGE than in other AEROCOM models. *Nho-Kim et al.* [2003] validated MOCAGE simulations of BC, comparing simulations with surface observations. Dust burden is lower in MOCAGE than in AEROCOM models, presumably the result of the MOCAGE dry deposition and sedimentation fluxes, which are stronger than those simulated by AEROCOM models, on average. However, *Martet et al.* [2009] validated the MOCAGE representation of mineral dust by comparing simulations with satellite data (Moderate Resolution Imaging Spectroradiometer; MODIS), light detecting and ranging data (AErosol RObotic NETwork), and station measurements (Interagency Monitoring of Protected Visual Environments network). Sulfate burden simulated by MOCAGE is similar to the higher estimate from the AEROCOM intercomparison. Dry deposition of this aerosol is of the same order of magnitude in MOCAGE as in AEROCOM models, whereas sulfate chemistry production simulated by MOCAGE is lower than in other AEROCOM models. High sulfate burden simulated by MOCAGE may be due to the wet deposition, which is less efficient in MOCAGE than in the other models, on average. *Ménégoz et al.* [2009] compared a MOCAGE simulation of sulfate with observations of the European Monitoring and Evaluation Programme [*Hjellbrekke*, 2004) and confirmed that MOCAGE tends to underestimate scavenging fluxes of sulfate. Nevertheless, this study shows that despite a slight tendency to overestimate sulfate concentration, MOCAGE describes rather well the distribution of sulfate over Europe.

2.5. Aerosol Budget Over the North Atlantic Region

[11] Figure 1 shows the main sinks and sources over the North Atlantic region for sulfate, BC, and mineral dust. Sulfate originates essentially from SO_2 oxidation, by an aqueous chemistry pathway, whereas gaseous chemistry

Table 2. Global Burden, Sinks, and Sources by MOCAGE and AEROCOM Models[a]

	Sulfate		Black Carbon		Mineral Dust	
	MOCAGE	AEROCOM	MOCAGE	AEROCOM	MOCAGE	AEROCOM
Burden	1.15	0.7 (0.3–1.2)	0.2	0.2 (0.11–0.37)	13.2	21.3 (6–30)
Emission + chem. prod. (sulfate only)	44.0	54 (30–80)	7.8	7.8 (-)	1670	1670 (-)
Dry deposition + sedimentation	6.6	6.8 (1–13)	3.2	1.6 (0.2–2.4)	1254	1120 (700–2100)
Wet deposition	37.2	47 (28–116)	4.5	6.2 (5.3–11)	427	498 (100–750)

[a]Burden is in Tg[S] for sulfate and Tg for other aerosols; sources are in Tg[S] yr^{-1} for sulfate and in Tg yr^{-1} for other aerosols. The mean and intervals of the MOCAGE and AEROCOM models are adapted from *Textor et al.* [2006]. Simulations are made with the same emissions for all AEROCOM and MOCAGE models in 2000.

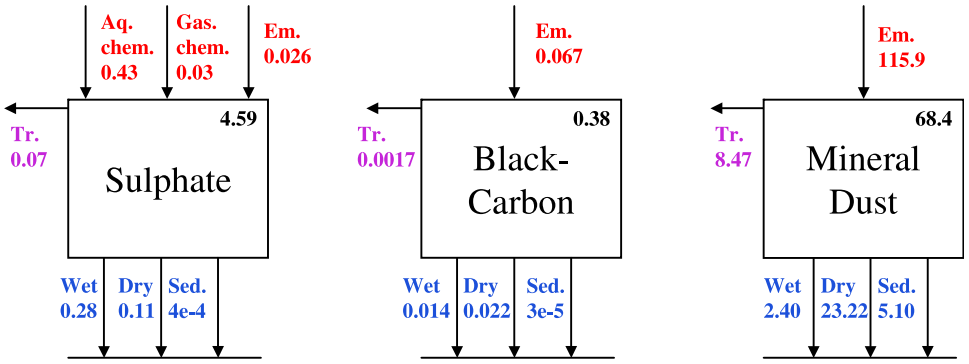

Figure 1. Sulfate, black carbon, and mineral dust budget over the North Atlantic region (20°N–80°N, 80°W–40°E) in winter (December–February) from 2000 to 2005. Burdens (top right corner of the square) are given in mg[S] m^{-2} for sulfate and in mg m^{-2} for the other aerosols. Fluxes are given in mg[S] m^{-2} d^{-1} for sulfate and in mg m^{-2} d^{-1} for the other aerosols. Tr., transport outside of the domain; Wet, wet deposition; Dry, dry deposition; Sed., sedimentation; Aq. chem., aqueous chemistry; Gas. chem., gaseous chemistry; Em., emissions.

pathways and direct emissions represent only 6% and 5% of total sulfate sources, respectively. Considering the north Atlantic region, the main sink for sulfate is wet deposition (0.28 mg[S] m^{-2} d^{-1}), followed by dry deposition (0.11 mg [S] m^{-2} d^{-1}) and transport outside of the domain (0.07 mg [S] m^{-2} d^{-1}). Sedimentation is negligible for sulfate, because of the very small size of this aerosol. The mean sulfate burden is 4.59 mg[S] m^{-2} in this region. The mean BC burden is 0.38 mg m^{-2}. The BC emissions, issued from biomass burning and human activities in Europe, Africa, and America, average 0.067 mg m^{-2} d^{-1} over the entire North Atlantic region. The main sink for this aerosol is dry deposition (0.022 mg m^{-2} d^{-1}), followed by wet deposition (0.014 mg m^{-2} d^{-1}) and export out of the domain (0.0017 mg m^{-2} d^{-1}). Sedimentation is negligible for BC, because of the small size of this aerosol. The mineral dust burden is 68.4 mg m^{-2} over the NAE region, with emissions coming from African and Middle East deserts equal to 115.9 mg m^{-2} d^{-1}, on average, over the whole domain. The main sinks for this aerosol are dry deposition (23.22 mg m^{-2} d^{-1}), followed by transport outside of the domain (8.47 mg m^{-2} day^{-1}), sedimentation (5.10 mg m^{-2} d^{-1}), and wet deposition (2.40 mg m^{-2} d^{-1}). The sum of all fluxes is equal to 0.026 mg[S] m^{-2} d^{-1} for sulfate, 0.029 mg m^{-2} d^{-1} for BC, and 76.7 mg m^{-2} d^{-1} for mineral dust. It is positive for all aerosols, indicating an accumulation of aerosols in the NAE region during the winter.

[12] Sulfate is essentially concentrated over Europe and America in winter, because of high SO_2 anthropogenic emissions (Figure 2a), the average burden varying between 5 and 9 mg[S] m^{-2}. Over the North Atlantic Ocean, the sulfate burden varies from 0 mg[S] m^{-2} in the tropics to 5 mg[S] m^{-2} in the north. Over Greenland, sulfate column load (i.e., burden) is very low (i.e., about 2 mg[S] m^{-2}). BC has a distribution similar to this of sulfate, with an averaged column load reaching 0.8 mg m^{-2} over Europe and America, 0.4 mg m^{-2} above the Atlantic, and 0.2 mg m^{-2} over Greenland (Figure 2b). There is, however, a large difference between BC and sulfate distributions over Africa: the sulfate burden is very low over this region, whereas the BC burden is comparable to that modeled in European polluted areas, because of strong biomass burning emissions in central Africa. Mineral dust is essentially concentrated over northern Africa, attributable to Saharan and Middle East desert emissions (Figure 2c). The winter average of dust column load varies between 200 and 500 mg m^{-2} above Africa, between 10 and 25 mg m^{-2} over Europe, and between 0 and 10 mg m^{-2} above the Atlantic Ocean and America. Only over the eastern part of the Atlantic is there a high concentration of dust: dust column load ranges from 200 mg m^{-2} in the West Coast of Africa to 0 mg m^{-2} in the middle of the North Atlantic region.

[13] The resulting aerosol radiative forcing is estimated by using aerosol optical thickness (AOT). AOT is computed here from the aerosol column load of sulfate, BC, and dust with the coefficients estimated by *Tegen et al.* [1997]. Figure 2d shows that simulated AOT takes very high values over Africa, reaching 0.6, because of the extreme concentration of mineral dust in the atmosphere. AOT ranges from 0.2 to 0.3 over Eastern Europe and from 0.1 to 0.2 over Western Europe, because of the presence of mineral dust, sulfate, and BC. Over America, AOT varies between 0.2 and 0.25, mainly because of the presence of sulfate and BC. AOT is between 0.1 and 0.15 over the Atlantic Ocean, except near the African western coast, where it can reach values of 0.4 because of the transport of desert dust. AOT takes its lower values over Greenland and over the Caribbean Sea, ranging from 0.05 to 0.01.

[14] In the study by *Tegen et al.* [1997], AOT is also computed with a CTM. It is generally lower than those simulated in this study over the continents: it does not exceed 0.3 over Africa and 0.016 over Europe and America. The same difference is noticed over the ocean, with AOT varying between 0.08 in the northern Atlantic and 0.2 in the tropical Atlantic in the study by *Tegen et al.* [1997]. In our study, we do not consider organic and sea-salt aerosols since they are not yet implemented in our model. It is then surprising that the AOT values of *Tegen et al.* [1997] are lower than ours, because they consider all the aerosols in their study. However, from comparisons with sun photometer measurements and satellite retrievals, *Tegen et al.*

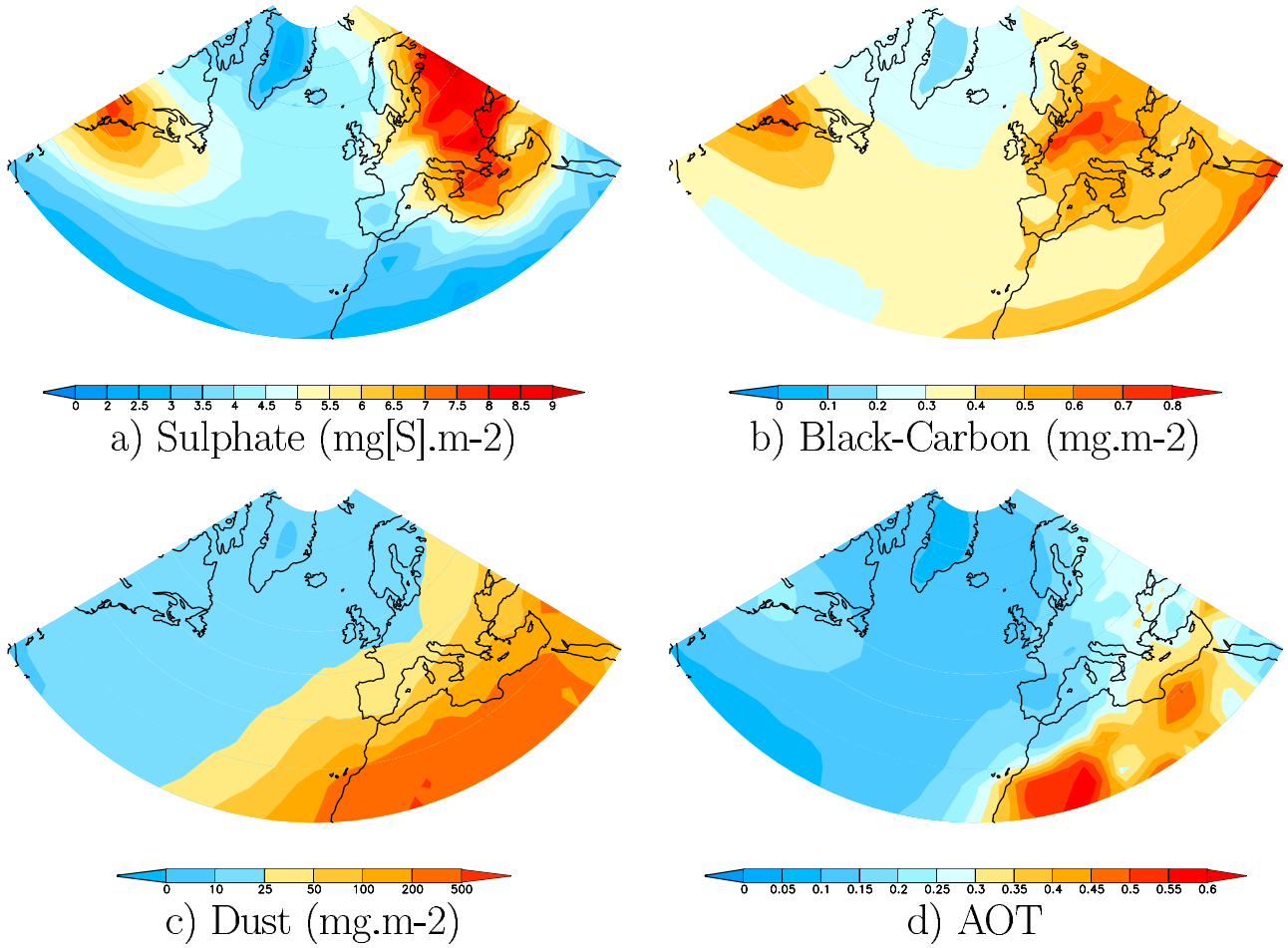

Figure 2. Sulfate (mg[S] m^{-2}), black carbon (mg m^{-2}), dust (mg m^{-2}), and aerosol optical thickness (AOT) winter average from 2000 to 2005 simulated by MOCAGE.

[1997] indicated that the AOT modeled in their study was often underestimated, in particular over Africa and Europe.

[15] *Remer et al.* [2008] evaluated AOT by analyzing MODIS satellite images. They evaluate a set of 5 year monthly means of AOT at a global scale. In that study, AOT in winter ranges between 0.1 and 0.3 over Europe, between 0.1 and 0.2 over the north of the Atlantic Ocean, except near the African western coast where it can reach 0.4, and from 0 to 0.15 over the American eastern coast. Theses values are of the same order of magnitude as those simulated by MOCAGE, which suggests that AOT distribution modeled by MOCAGE is quite realistic.

3. Aerosol Distribution Induced by North Atlantic European Weather Regimes

3.1. Weather Regime Classification

[16] The MOCAGE simulation is driven using operational analysis products. However, the 2000–2005 period is too short to define robust cluster centroids. We have thus classified MOCAGE data onto the four weather regimes obtained from the 1958–2001 ERA40 reanalysis product [*Gibson et al.*, 1997; *Uppala et al.*, 2004]. The classification is applied to the 500 hPa geopotential height (Z500) over the North Atlantic European region (20°N–80°N, 80°W–40°E). An empirical orthogonal function (EOF) analysis is performed on the daily anomalies of Z500 for the winter (December–February; DJF) season. The first 30 EOFs are retained, capturing more than 90% of the total variance. The decomposition of the large-scale atmospheric circulation variability into weather regimes is performed in the space spanned by the leading EOFs, using the *k*-means partition algorithm developed by *Michelangeli et al.* [1995]. As described by *Michelangeli et al.* [1995], *k* was chosen to be 4, and hence the daily anomalies of Z500 were classified into four clusters, which constitute the optimal partition, compared with a classification performed on a multivariate noise.

[17] The four weather regimes from the ERA40 reanalysis obtained following this method are represented in Figure 3. The first regime (Figure 3a), named the zonal regime, consists of a dipole of anomalies with a negative center covering the northern North Atlantic Ocean, situated north of a positive center extending from the eastern American coast to the southern European continent. This regime corresponds to the positive phase of the North Atlantic Oscillation (NAO–). The colored areas correspond to anomalies significant at the 95% level, according to a bootstrap test. The second regime (Figure 3b), named the blocking regime, displays an anomalous ridge centered

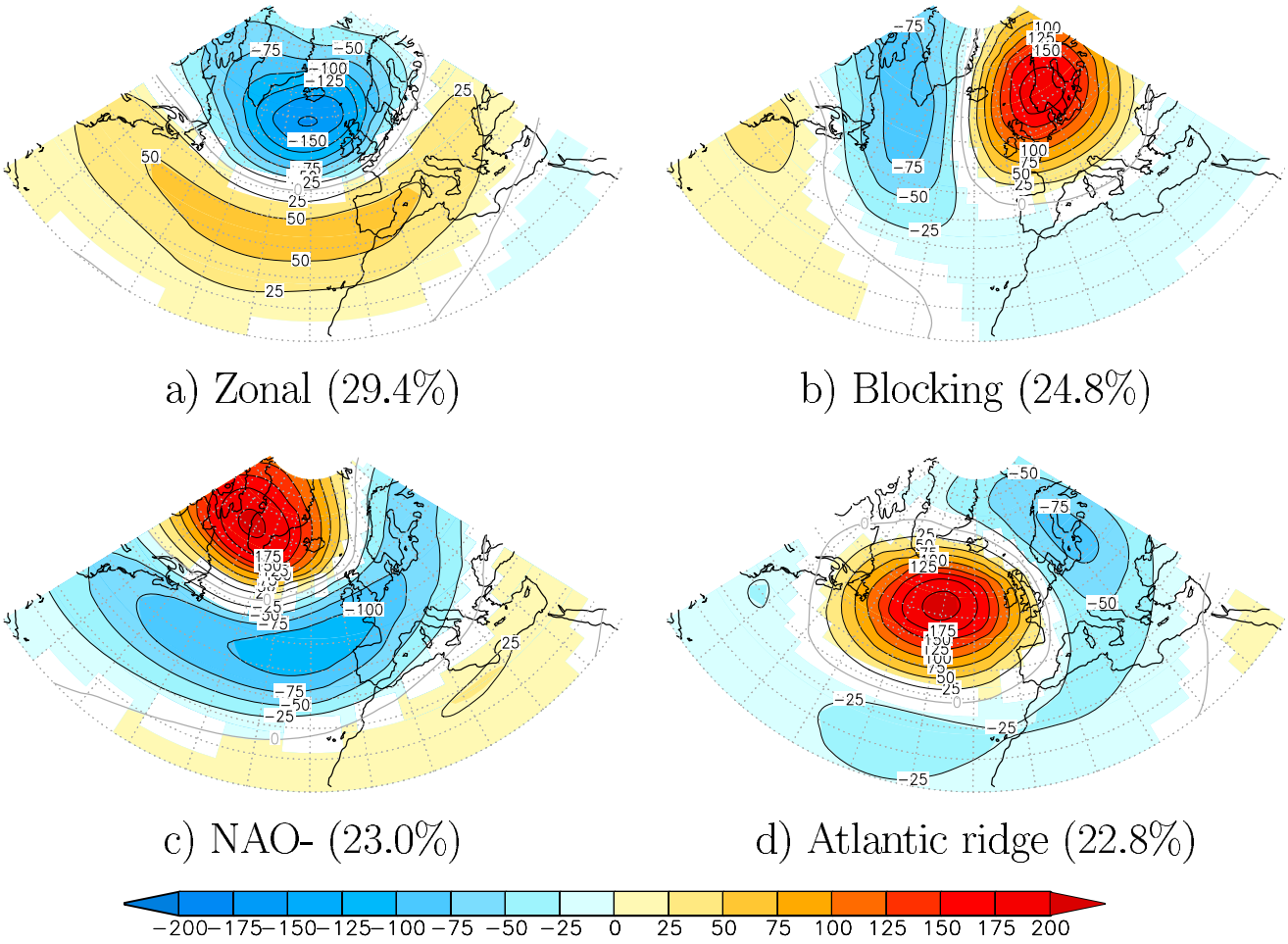

Figure 3. Composites of the anomalies of ERA40 500 hPa geopotential height anomalies (m) corresponding to the four North Atlantic weather regimes in winter (December–February): (a) zonal; (b) blocking; (c) NAO–; (d) Atlantic ridge. Weather regime frequencies are in parentheses. The contour interval is 25 m; 95% significant values are shown in color.

over the Scandinavian Peninsula, along with a trough extending southward from the Baffin Bay. The third regime (Figure 3c), named NAO– (negative NAO phase), consists of a dipole of anomalies with a positive center over the southern coast of Greenland and a negative center over the Azores Islands. The Atlantic ridge regime (Figure 3d) is dominated by an anticyclonic anomalous core off Western Europe flanked to the northeast by a low pressure center over the Scandinavian peninsula.

[18] The daily operational analysis of the 2000–2005 period used in our MOCAGE simulation is classified in terms of the weather regimes already defined. Before performing the classification, the daily anomalies of Z500 for the DJF season, are projected onto the first 30 EOFs computed from the ERA40 reanalysis. Each day is attributed to the class for which the Euclidian distance with the cluster centroid from ERA40 reanalysis is minimal. The classification in weather regimes is thus achieved in the space spanned by the leading 30 EOFs of the ERA40 reanalysis.

[19] In MOCAGE simulations, all meteorological variables are provided from analyses of the ECMWF IFS model, except convective precipitation flux, which is computed by MOCAGE. Figures 4 and 5 show precipitation and wind anomalies associated with each weather regime. Precipitation anomalies are obtained from the classification of the total precipitation flux, which is the sum of a stratiform component issued from the IFS model and a convective component computed in MOCAGE. Wind anomalies originate from a classification of the IFS model analyses.

[20] The zonal regime is characterized by a low-pressure system over the north of the domain, inducing a northward shift of the storm track and therefore more precipitation over northern Europe and less precipitation over southern Europe (Figure 4a). In contrast, the NAO– regime induces a southward shift of the storm track, associated with less precipitation over northern Europe and more precipitation over southern Europe (Figure 4c). The blocking regime induces a deviation of the storm track toward the northern North Atlantic Ocean, associated with fewer storms reaching northern Europe. The blocking regime is therefore characterized by less precipitation over Europe and more precipitation over the Atlantic (Figure 4b). Finally, the Atlantic ridge induces a slowdown of the westerly flow and then less precipitation in the

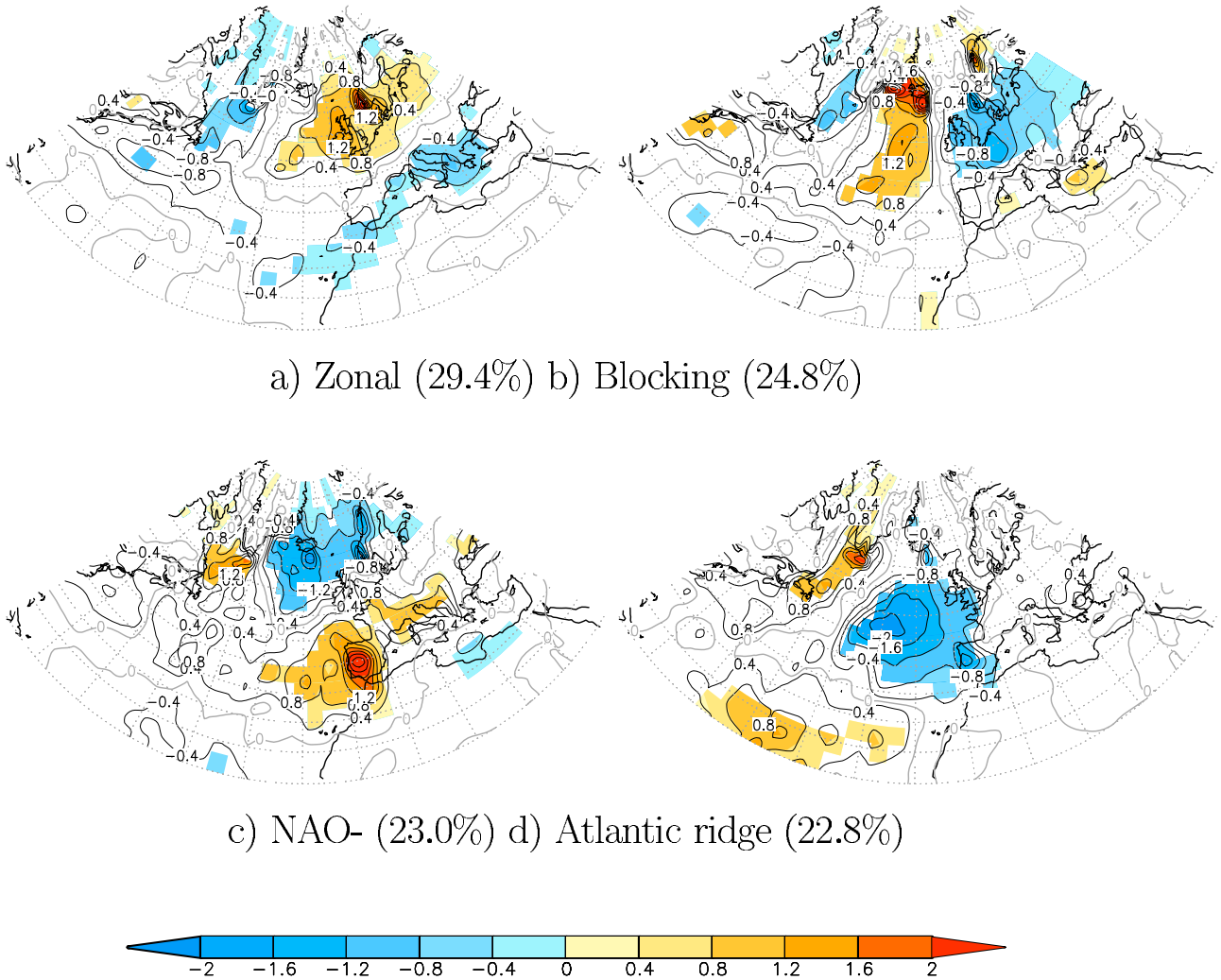

Figure 4. Composites of 2000–2005 ECMWF/MOCAGE (see text for description) liquid precipitation anomalies (mm d^{-1}) during the days for which the atmosphere is classified as (a) zonal, (b) blocking, (c) NAO–, or (d) Atlantic ridge,. The contour interval is 0.4; 95% significant values are shown in color.

northeastern Atlantic Ocean (Figure 4d). The zonal regime is associated with an increased cyclonic circulation in the north of 45°N (Figure 3a), contrary to the NAO– regime, which is characterized by an increased anticyclonic circulation in the same region (Figure 5c). The blocking regime is characterized by stronger southerly winds over the northern North Atlantic Ocean (Figure 5b). The high-pressure system over the ocean during an Atlantic ridge episode induces strong northerly winds on the western coast of Europe and Africa (Figure 5d). The meteorological field variations associated with each weather regime over the North Atlantic basin are expected to have an impact on aerosol concentrations, through the modification of chemical production, deposition, and transport of aerosols. These links between the weather regimes and the aerosol distribution are investigated in sections 3.2–3.6.

3.2. Aerosol Budget Variations Associated With Weather Regimes

[21] The aerosol budget associated with each weather regime (Table 3) is computed as a composite of the days for which MOCAGE data are classified as pertaining to this weather regime. We have to keep in mind that we used climatologic dust emissions in our simulation, which do not depend on wind velocities. The representation of dynamical dust emissions is not yet implemented in the version of the model used here. Considering our simulation, we analyze only aerosol burden variations linked to transport and sinks efficiency (except for sulfate sources, which are described by chemical reactions, which depend also on meteorological conditions).

[22] Averaged over the entire NAE region, the differences in the aerosol budget simulated for each weather regime are relatively small: the mean sulfate burden over the North Atlantic region varies by about 5% depending on the weather regime relative to the winter mean. These variations are the result of changes in export of sulfate out of the NAE region and variations of wet deposition, dry deposition, and aqueous and gaseous chemistry production. The export of sulfate out of the NAE region can be modified by a factor 10 depending on the weather regime considered, whereas the variations of the other fluxes do

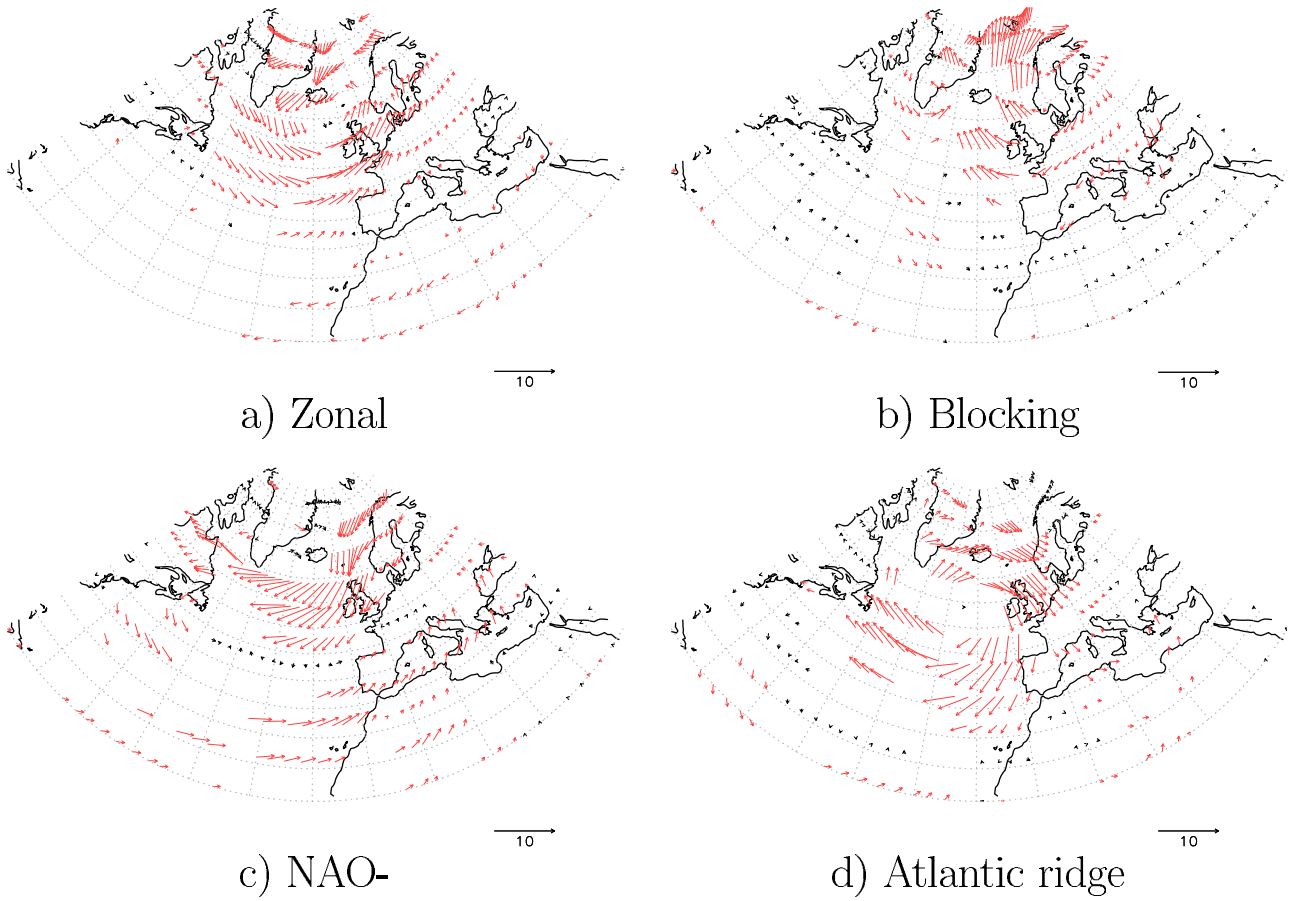

Figure 5. Composites of 2000–2005 ECMWF IFS model (see text for description) wind anomalies (m s^{-1}) during the days for which the atmosphere is classified as (a) zonal, (b) blocking, (c) NAO–, or (d) Atlantic ridge. The 95% significant values are shown in red.

not exceed 10%. The BC burden varies by less than 3%, and dry and wet deposition (its two main sinks) vary by no more than 5%, depending on the weather regime considered. The mean dust burden undergoes variations by up to 10%, depending on the weather regime considered. This is induced by changes in transport outside of the domain, sedimentation, and wet and dry deposition, which can vary by 15% from one weather regime to another for this aerosol.

[23] To evaluate the local differences of the aerosol burden, we computed the composites of burden, sinks, and sources of aerosols associated with each weather regime. The patterns obtained are described in percentages in Figures 6–9 and are discussed in the following.

3.3. Zonal Regime Signature

[24] The zonal weather regime induces significant negative anomalies of the sulfate column load all over Europe (Figure 6a), reaching 15% (−1.2 mg[S] m^{-2}). The zonal regime is associated with more precipitation (Figure 2a) and therefore a moister atmosphere over northern Europe. For this reason, the aqueous chemical production is increased over northern Europe (compare with Figure 6g). Nevertheless, reinforced southwesterly winds transport sulfate produced over Europe toward northern Europe, a very humid region, leading to a strong increase in wet deposition (Figure 6g). This mechanism implies a general decrease in the sulfate burden over Europe. A slight sulfate burden increase is modeled over northern Africa, because of an increase in aqueous chemistry that is not compensated by an increase in wet deposition over this region. A significant negative anomaly of BC column load is modeled over western Europe during zonal regime episodes: a negative anomaly of 20% (−0.1 mg m^{-2}) is modeled, in particular, over England (Figure 6b). Two reasons explain such a decrease: more intense precipitation reinforces wet deposition over western Europe, and increased northward winds (see Figure 3a) transport BC from highly polluted areas in western Europe (see Figure 5b) to northern Europe, where wet deposition is very efficient because of high precipitation rates. The zonal regime is also associated with a strong negative anomaly of mineral dust burden, reaching 25% (with values up to −70 mg m^{-2}), over a region extending from northern Africa to the Black Sea (Figure 6c). This negative anomaly is explained by the increase in easterly winds associated with the zonal regime (Figure 3a), inducing also a strong positive anomaly over the oceanic region located in the west coast of Africa. The negative anomaly of dust modeled over northern Europe (Figure 6c), varying between 10% and 25% (not exceeding 10 mg m^{-2} in absolute value), is linked to a positive anomaly of wet deposition (Figure 6h). The AOT model is a combination of

Table 3. Sinks and Burden of Sulfate, Black Carbon, and Mineral Dust Over the North Atlantic Region (20°N–80°N, 80°W–40°E) in Winter (December–February) 2000–2005 Associated With the Four Weather Regimes: Zonal, Blocking, NAO–, and Atlantic Ridge[a]

	Weather Regime			
	Zonal	Blocking	NAO–	Atlantic Ridge
Sulfate (mg[S] m^{-2} d^{-1}, mg[S] m^{-2})				
Wet deposition	0.289	0.267	0.290	0.280
Dry deposition	0.107	0.114	0.115	0.110
Sedimentation	–	–	–	–
Transport	−0.23	0.84	−0.53	−0.42
Aqueous chemistry	0.441	0.410	0.455	0.450
Gaseous chemistry	0.031	0.029	0.026	0.029
Burden	4.419	4.709	4.714	4.659
Black carbon (mg m^{-2} d^{-1}, mg m^{-2})				
Wet deposition	0.0145	0.0142	0.0149	0.0136
Dry deposition	0.0208	0.0232	0.0210	0.0212
Sedimentation	–	–	–	–
Transport	−0.0022	−0.0007	−0.0016	−0.0022
Burden	0.367	0.391	0.387	0.387
Dust (mg m^{-2} d^{-1}, mg m^{-2})				
Wet deposition	2.05	2.65	2.31	2.98
Dry deposition	23.05	22.74	22.78	23.23
Sedimentation	5.12	5.02	5.03	5.07
Transport	−9.22	−7.24	−7.85	−8.42
Burden	63.67	70.72	66.54	75.64

[a]Transport is positive when turned inside the NAE region.

the three aerosol burdens taken into account in our simulation. The zonal regime is therefore associated with significant AOT negative anomaly over Europe and northern Africa. A slight AOT negative anomaly is also pointed out over the North Atlantic Ocean. There is an intense positive anomaly over the ocean along West Africa attributed to dust. During a zonal regime episode, the typical value of AOT decrease is 10% (from −0.02 to −0.07) over Africa and Europe, and the typical value of AOT increase is about 20% (from +0.01 to +0.06) over the West African coast.

3.4. Blocking Regime Signature

[25] The blocking regime is associated with an enhancement of 10% (+0.4 to +0.8 mg[S] m^{-2}) of the sulfate burden over southern Europe compared with the winter mean (Figure 7a). During this weather regime, the atmosphere is drier over polluted areas in central Europe, and aqueous chemical production is therefore less active (Figure 7g), but wet deposition is also less efficient (Figure 7e). Such a situation implies a decrease in the sulfate burden over Scandinavia, whereas combined with reinforced northerly winds (Figure 3b), it favors an increase in the sulfate burden modeled over the Mediterranean Sea. Negative anomalies modeled over Scandinavia are linked to strong southwesterly winds associated with the blocking regime (Figure 3b). The BC burden associated with the blocking regime is increased over western and southern Europe (by 10%–20%, i.e., +0.4 to +0.12 mg m^{-2}) (Figure 7b) and decreased over Scandinavia, essentially because of the atmospheric circulation induced by this regime. Northeasterly winds transport BC from northeastern Europe to western and southern Europe. This tendency is reinforced by low levels of wet deposition over northern Europe (Figure 7f). Weak dust anomalies are modeled for the blocking regime over two regions: negative anomalies from 10% to 40% (up to −10 mg m^{-2}) over the tropical Atlantic and positive anomalies between 30% and 50% (i.e., between +10 and +40 mg m^{-2}) over western Europe and northwestern Africa (Figure 7c). These anomalies are explained by wind anomalies associated with the blocking regime. The blocking regime is associated with AOT anomalies largely positive over all of western Europe (20% increase, i.e., +0.02) and negative over the Scandinavian region (10% decrease, i.e., −0.02) (Figure 7d).

3.5. NAO- Regime Signature

[26] The NAO– regime is associated with strong positive sulfate and BC anomalies over Europe (between 10% and 20% for sulfate, i.e., between +0.4 and +1.4 mg[S] m^{-2}; and between 5% and 10% for BC, i.e., between +0.04 and +0.08 mg m^{-2}-) and negative sulfate and BC anomalies over Africa (between 10% and 20% for sulfate, i.e., between −0.4 and −1.4 mg[S] m^{-2}; sulfate and around 5% for BC, i.e., up to −0.04 mg m^{-2} (see Figures 8a and 8b). The accumulation of sulfate over Europe, combined with a decrease in sulfate burden over the Mediterranean Sea and northern Africa, is probably linked with the atmospheric circulation (Figure 3c). Wind anomalies may limit the discharge of sulfate from Europe. Wet deposition and aqueous chemical production anomalies have a low level of significance over the NAE region during the NAO– phase (Figures 8e and 8g). However, an increase in aqueous chemistry production over Europe (Figure 8g), more intense than the increase in wet deposition modeled over this region (Figure 8e), could reinforce the accumulation of sulfate over the European continent. An accumulation of sulfate is also modeled over the tropical Atlantic, about 10% (from +0.2 to +0.6 mg[S] m^{-2}), linked to a southward shift of westerlies, which transport both sulfate and SO_2 over this region. For this reason, aqueous chemistry is also reinforced in this region (Figure 8g). The BC burden is also accumulated over Scandinavia, with anomalies between 5% and 10% (i.e., between +0.02 and +0.08 mg m^{-2}), because of a decrease in wet deposition. Over the western tropical Atlantic, reinforced westerlies imply slight BC positive anomalies. Negative dust anomalies reaching 50% (up to +70 mg m^{-2}) are noticed over the Atlantic Ocean, close to Africa, because of a decrease in the easterlies that limit the transport of dust from the Sahara to the Atlantic Ocean. This process also explains the dust positive anomaly modeled over North Africa. As a consequence of these aerosol burden anomalies, the NAO– regime signature in AOT is characterized by a negative anomaly near the western African coast (reaching a 40% decrease, up to −0.07), linked to low dust burden, and by two positive anomalies over the western tropical Atlantic (10% increase, i.e., +0.01) and northern Europe (20% increase, from +0.01 to +0.04), linked to strong accumulations of sulfate and BC.

3.6. Atlantic Ridge Signature

[27] The Atlantic ridge signature in sulfate burden is characterized by negative anomalies over the center of the North Atlantic Ocean and northwestern Europe, with

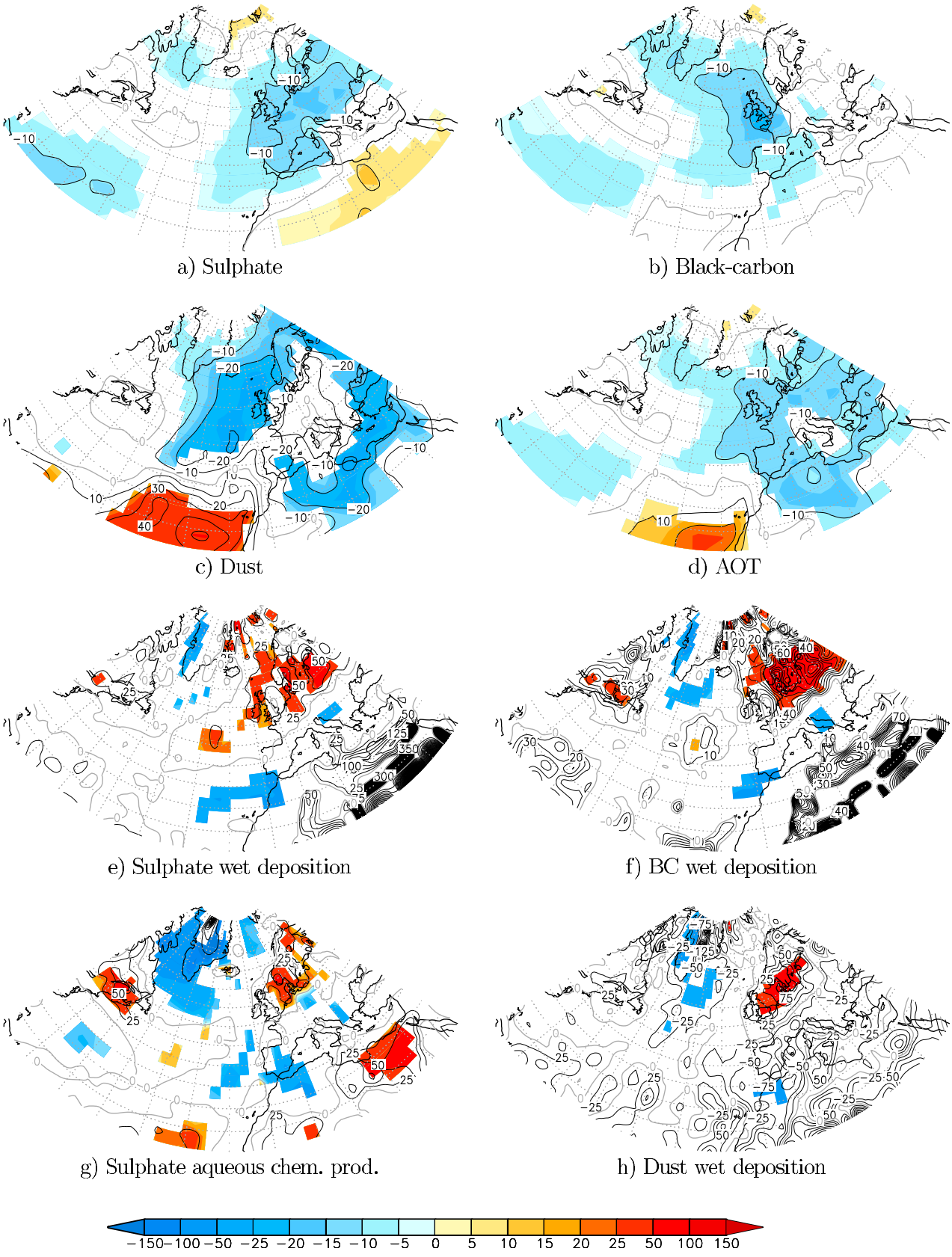

Figure 6. The 2000–2005 DJF zonal regime anomalies (in percentage) of sulfate burden, black carbon (BC) burden, dust burden, aerosol optical thickness (AOT), sulfate wet deposition, BC wet deposition, sulfate aqueous chemical production, and dust wet deposition over the North Atlantic region; 95% significant values are shown in color.

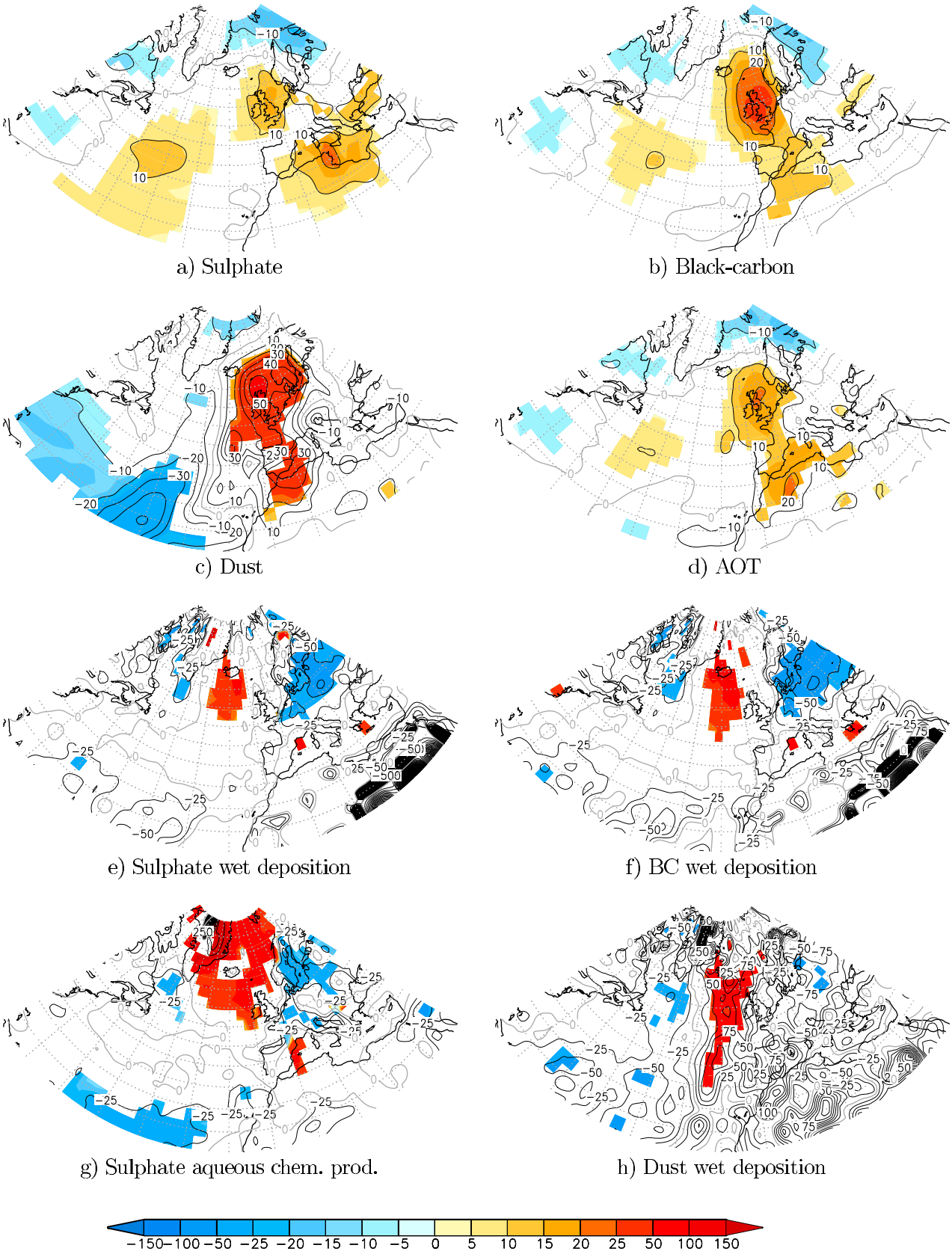

Figure 7. The 2000–2005 DJF blocking regime anomalies (in percentage) of sulfate burden, black carbon (BC) burden, dust burden, aerosol optical thickness (AOT), sulfate wet deposition, BC wet deposition, sulfate aqueous chemical production, and dust wet deposition over the North Atlantic region; 95% significant values are shown in color.

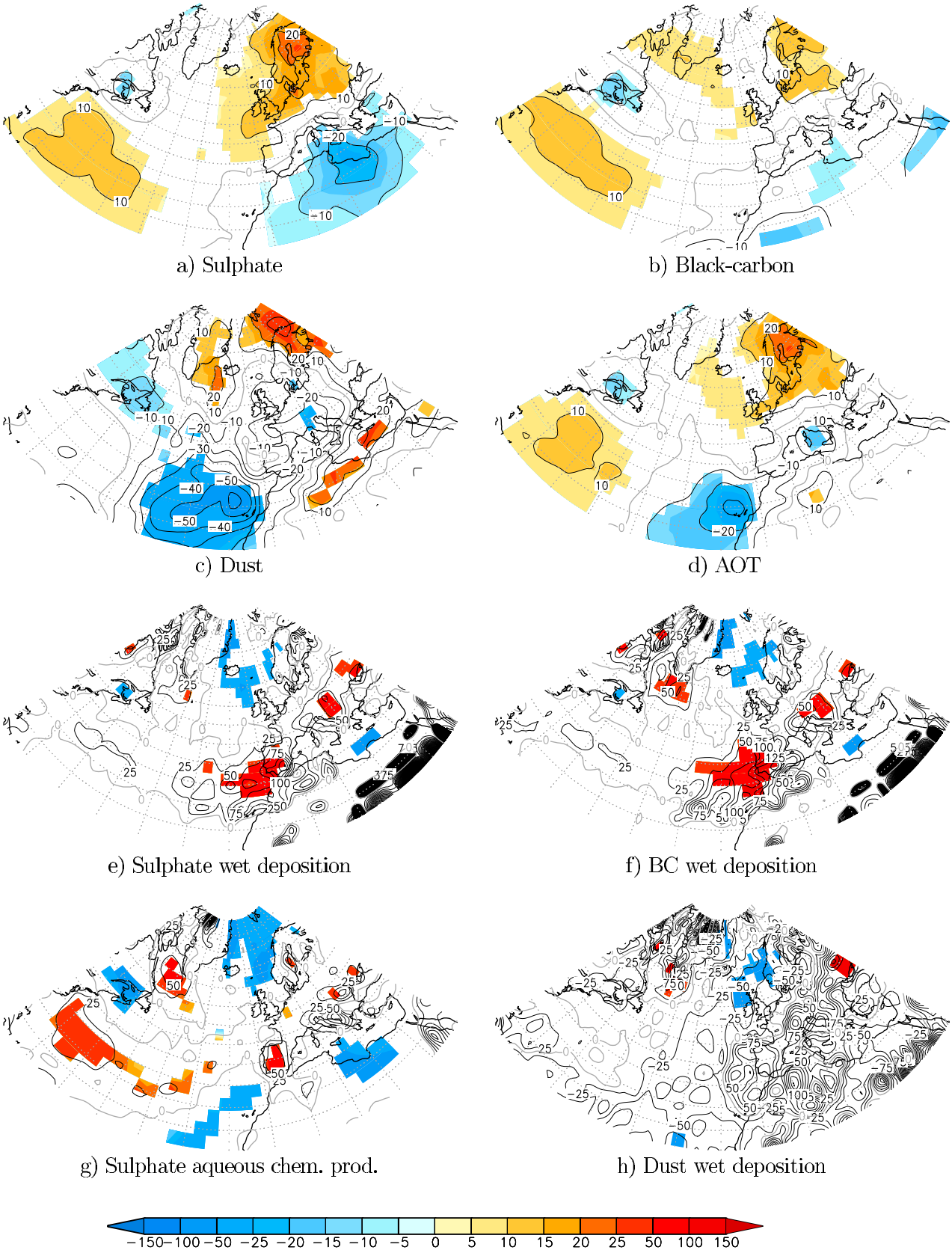

Figure 8. The 2000–2005 DJF NAO– regime anomalies (in percentage) of sulfate burden, black carbon (BC) burden, dust burden, aerosol optical thickness (AOT), sulfate wet deposition, BC wet deposition, sulfate aqueous chemical production, and dust wet deposition over the North Atlantic region; 95% significant values are drawn in color.

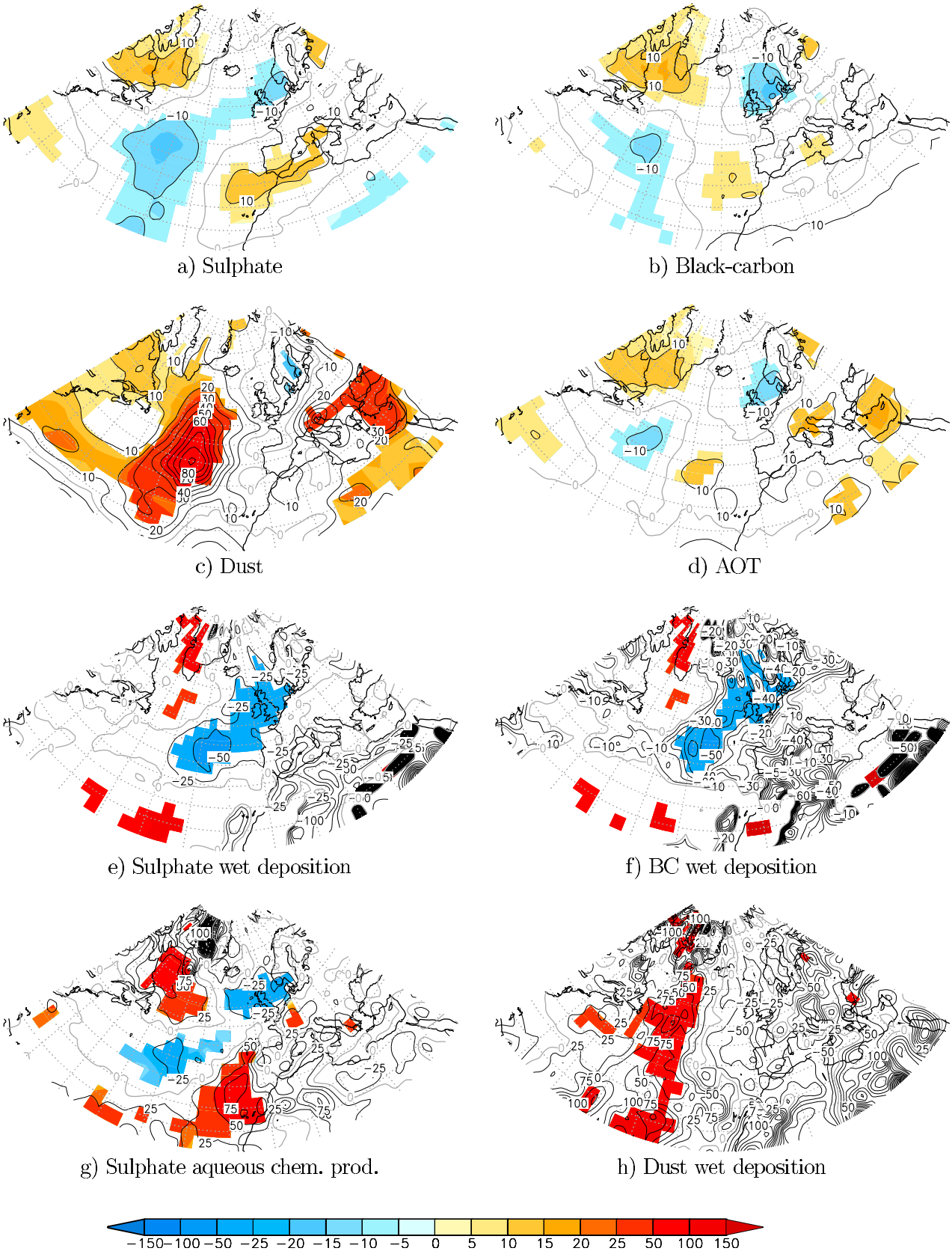

Figure 9. The 2000–2005 DJF Atlantic ridge regime anomalies (in percentage) of sulfate burden, black carbon (BC) burden, dust burden, aerosol optical thickness (AOT), sulfate wet deposition, BC wet deposition, sulfate aqueous chemical production, and dust wet deposition over the North Atlantic region; 95% significant values are shown in color.

values from 5% to 15% (from −0.2 to −0.6 mg[S] m^{-2}), and by positive anomalies over southwestern Europe and northern America, with values oscillating around 10% (from +0.02 to +0.06 mg[S] m^{-2}) (Figure 9a). The positive anomalies over southwestern Europe are linked both to reduced westerly winds (Figure 3d) and to a more active aqueous chemical production over central and southwestern Europe (Figure 9g). Because of strong emissions of sulfur compounds in northern America, reduced westerly winds over the Atlantic Ocean induce a negative sulfate anomaly over the Atlantic Ocean and a positive sulfate anomaly over America. The sulfate wet deposition negative anomaly over the Atlantic Ocean is probably not caused by a change in meteorological conditions. But it may be associated directly with the decrease in sulfate concentration over this region. The negative anomaly of sulfate modeled in northwestern Europe is linked to positive anomalous northwesterly winds (Figure 3d). The BC burden shows a negative anomaly over the North Atlantic center from 5% to 15% (from −0.02 to −0.06 mg m^{-2}) and positive anomalies over western Europe and northern America reaching 15% (+0.04 mg m^{-2}) (Figure 9b). Such distribution anomalies are due to the Atlantic ridge wind anomalies (Figure 3d), inducing a transport of BC from northern to southwestern Europe. A strong positive dust anomaly with values between 10% and 30% (between 20 and 50 mg m^{-2}), modeled over eastern Africa, is linked with the increase in northwest winds (Figure 3d), transporting dust on the southwest of the NAE region. The AOT distribution associated with the Atlantic ridge regime is therefore characterized by positive anomalies over Africa and southern Europe (10% increase, up to +0.05) and negative anomalies over northwestern Europe (10% decrease, up to −0.01).

4. Feedback of the Aerosol Distribution on the Weather Regimes

[28] It was shown in section 3 that weather regimes can significantly affect the aerosol burden. A new question arises from this result: Can aerosol burden, in turn, exert an influence on weather regimes? To assess the impact of these aerosol burden anomaly patterns, experiments are conducted in which an AGCM is forced by the North Atlantic aerosol burden anomalies shown in Figures 6–9.

4.1. ARPEGE Global Climate Model

[29] The atmospheric model used for these experiments is the ARPEGE-Climat version 4 AGCM [*Déqué et al.*, 1999; *Gibelin and Déqué*, 2003]. The model has 31 vertical levels extending up to 10 hPa by using a hybrid sigma-pressure vertical coordinate and a 2.8° horizontal resolution. The semi-Lagrangian advection scheme allows for a 30 min time step. The Interaction Sol-Biosphère-Atmosphère (ISBA) Soil-Vegetation-Atmosphere Transfer model, described by *Mahfouf et al.* [1995] is included in ARPEGE-Climat, which also contains a snow cover formulation [*Douville et al.*, 1995a, 1995b]. Soil and vegetation properties are prescribed from the global high-resolution ECOCLIMAP data set [*Masson et al.*, 2003]. The radiative scheme used in ARPEGE is the Fouquart-Morcrette Radiation scheme [*Dandin and Morcrette*, 1996], describing the absorption and emission in the longwave radiation and reflection, scattering, and absorption in the solar radiation. Two wide wave bands (0.25–0.68 μm and 0.68–0.4 μm) are used in the shortwave radiation calculation. Reflection, scattering, and absorption by gases, aerosols, and clouds are computed by applying a two-stream method together with a photon path distribution method [*Fouquart and Bonnel*, 1980]. Longwave radiation is computed by a broadband flux emissivity method with six wide wave bands covering the spectrum between 0 and 2620 cm^{-1} without the scattering process.

[30] The direct effect of the aerosols, i.e., their aptitude to scatter and to absorb solar radiation, is taken into account in ARPEGE-Climat as presented by *Rongming et al.* [2001]. The model is based on vertically integrated AOT, a single scattering albedo, and an asymmetry factor for each aerosol. Representation of these parameters was originally done according to the works by *Tanré et al.* [1984] and *Dandin and Morcrette* [1996]. Six types of aerosols are presently considered in ARPEGE-Climat simulations: BC, dust, sulfate, OC, sea salt, and volcanic and stratospheric background aerosols. For each type of aerosol, a specific vertical profile is applied to "verticalize" 2-D AOT inputs (see Figure 10). In our simulation, BC, dust and sulfate AOT monthly means were computed from our 2000–2005 MOCAGE simulation: MOCAGE aerosol burdens were vertically integrated and then converted into 2-D AOT after a linear transformation as described by *Tegen et al.* [1997]. It would have been interesting to directly use 3-D AOT from MOCAGE in ARPEGE, but that could not be done easily for this study. Furthermore, MOCAGE does not describe sea salt and OC at the present, so for these aerosols we used the monthly mean AOT estimated by *Tegen et al.* [1997]. Background aerosols concern both volcanic aerosols that penetrate into the stratosphere and sulfate aerosols issued from the oxidation of carbonyl sulfide, a compound that is chemically inert on the troposphere but is oxidized into sulfate in the stratosphere [*Turco et al.*, 1980]. In our simulation, the 2-D AOT inputs for these two aerosols are constant, both spatially and temporally. They are taken from work by *Tanré et al.* [1984].

[31] An increase in sulfate aerosol can increase the number of cloud condensation nuclei taken in a constant cloud liquid water content; this leads to a larger concentration of cloud droplets of small radius and then to an enhancement of cloud reflectivity [*Twomey*, 1977]. This effect, named "first indirect effect, " is very difficult to quantify and has been discussed many times [*IPCC*, 2007; *Heintzenberg and Charlson*, 2009]. Moreover, global climate model resolution is often too coarse to describe this effect correctly. However, one single relationship between sulfate concentration and cloud droplet number concentration (CDN) is classically used for climate study [*Boucher and Lohmann*, 1995]:

$$C_{\mathrm{dn}} = 10^{a+b[\log(\mathrm{mSO}_4^{2-})]}, \quad (1)$$

where mSO_4^{2-} is the sulfate mass expressed in $\mu g\ m^{-3}$ and C_{dn} is CDN expressed in cm^{-3}.

[32] Many different values of a and b coefficients have been proposed. In our ARPEGE-Climat simulations, we used those recently updated by J. Quaas (MPI, Hamburg, Germany, personal communication, 2005): $a = 1.7$ and $b =$

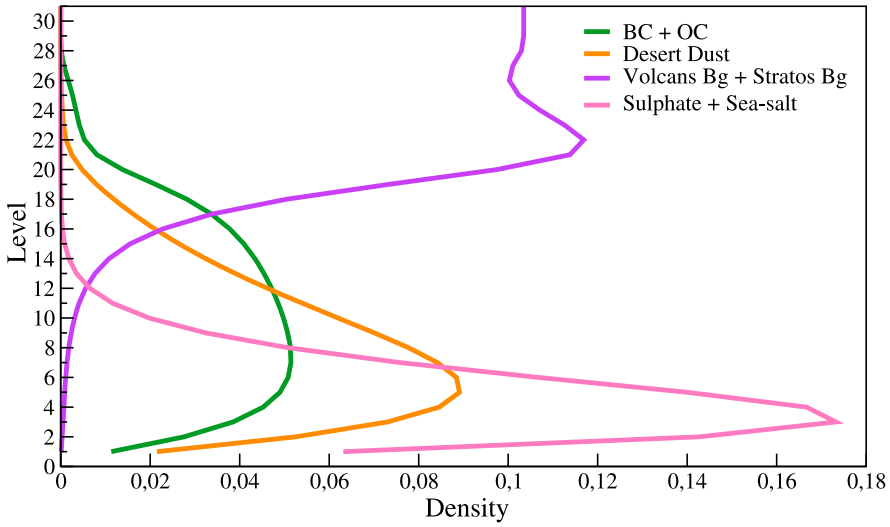

Figure 10. Aerosol profiles prescribed in the 31-level ARPEGE-Climat model.

0.2. In ARPEGE-Climat, computation of the effective radius of cloud liquid water droplets and then the AOT, the asymmetry factor, and the single scattering albedo of clouds, all depending on the CDN, liquid water content, and liquid water path, is done as described by *Rongming et al.* [2001].

4.2. Atmosphere-Forced Experiments

[33] Five experiments are conducted: one control experiment (CTL), using an average AOT value from the CTM simulation, and four experiments to test the sensitivity of the atmosphere to the pattern of aerosol burden associated with each weather regime in the 20°N–80°N, 80°W–40°E domain. These experiments are forced with the anomaly patterns of aerosols associated with the zonal, blocking, Atlantic ridge, and NAO– regimes. They are, respectively, named AER-ZO, AER-BL, AER-AR, and AER-NAO. The CTL experiment is forced with a monthly climatology of aerosols, computed as the monthly mean of the 2000–2005 MOCAGE simulation presented in section 2.3. In the other four experiments, the aerosol fields are computed by adding the aerosol anomaly patterns (Figures 6–9) to the 2000–2005 monthly mean used in the CTL experiment. Note that the AOT anomalies taken into account are induced only by BC, dust, and sulfate anomalies. Since MOCAGE cannot simulate the evolution of sea salt and OC, it was not possible to evaluate the AOT anomalies induced by the variations of these aerosol burdens associated with each weather regime. Then, the AOT of sea-salt and OC aerosols is the same in all the experiments. Each of these five experiments consists of an ensemble of 50 simulations of the winter (DJF) season, starting from 50 different initial conditions for 1 December. The greenhouse gases are arbitrarily fixed to their 1990 values. These values are the same for all the ensemble of simulations, because only the impact of aerosol variations is being studied here. The monthly climatology sea-surface temperature of *Reynolds et al.* [2002] is prescribed as surface boundary conditions, with a conservative quadratic interpolation between consecutive months.

4.3. Impact of the Aerosol Distribution on the Weather Regime Persistence

[34] The daily large-scale atmospheric circulation from these five experiments is classified into the four weather regimes obtained from the ERA40 reanalysis. The method is the same as the one used to classify MOCAGE data. We consider as weather regime episodes those lasting at least 3 consecutive days, as considered by *Sanchez-Gomez and Terray* [2005]. This hypothesis is justified by the persistence properties of the weather regimes [*Michelangeli et al.*,1995]. The excitation and associated transitions of the four weather regimes are mainly controlled by internal atmospheric dynamical processes, but external forcings are expected to stabilize or destabilize the atmospheric circulation state. The potential role of aerosol concentration anomalies is assessed by evaluating the ability of such anomolies to influence the mean persistence of each weather regime.

[35] First of all, no differences are detected between the experiments, neither in the frequency of occurrence, nor in the spatial characteristics of the weather regimes. We only detect differences in the persistence of weather regimes. From the four sensitivity tests AER-ZO, AER-BL, AER-NAO, and AER-AR, several impacts of aerosol distribution on weather regime persistence were pointed out. Some of them are not significant according to a two-sided bootstrap test and therefore are not presented here. Two of them were found to be significant and are described below.

[36] We find that the mean persistence of the NAO– regime is reduced by 1.78 days when the atmosphere is forced with the pattern of aerosol induced by the zonal regime instead of the climatology (CTL) with a p value equal to 0.086 according to our two-sided test. This diminution represents 20% of the mean persistence of the NAO– regime, which is equal to 9.0 days in the CTL experiment. During an occurrence of the zonal regime, the

pattern of aerosol anomalies named AER-ZO will be forced by the atmosphere. Then, if because of an internal atmospheric dynamical process a transition from the zonal regime to the NAO– regime is produced, the AER-ZO pattern will tend to destabilize the NAO– regime.

[37] The mean persistence of the zonal regime is reduced by 0.88 days when the atmosphere is forced with the pattern of aerosol induced by the blocking regime instead of the climatology (CTL) with a p value equal to 0.116 according to a two-sided test. This diminution represents 10% of the mean persistence of the zonal regime, which is equal to 8.6 days in the CTL experiment. Similarly, during a transition from the blocking regime to the zonal regime, the interaction with the aerosol will tend to destabilize the zonal regime.

4.4. Discussion

[38] As presented in section 3.4, the zonal regime is associated with strong negative anomalies of sulfate and BC over all of Europe (Figure 6). During the occurrence of this regime, dust burden takes negative anomalies over North Africa and positive anomalies above the Atlantic part that borders West Africa. The change in aerosol burden in the AER-ZO experiment has, directly or indirectly (through all climate feedback), an impact on the radiative fluxes modeled over the NAE region, as shown in Figure 11. This figure shows the difference between radiative fluxes simulated in the AER-ZO (made with the zonal aerosol distribution) and in the CTL (made with the standard winter average aerosol distribution) during the NAO– phase.

[39] Radiative flux anomalies cannot be linked easily to the pattern of the aerosol burden anomalies, because of the involvement of many climate retroactions, in particular those that concern cloud feedback. In our experiment, the solar radiation flux anomalies at the top and the bottom of the atmosphere (Figures 11a and 11b) have very low significance levels. However, the positive anomaly of surface solar radiation modeled over the Sahara (keep in mind that positive fluxes are oriented downward) is probably caused by the negative anomaly of dust burden associated with the zonal regime (Figure 6c). In west North Africa, a negative anomaly of surface solar radiation may be induced by both positive dust burden anomalies (Figure 6c) and positive cloud amount anomalies over this region (Figures 11e and 11f). Longwave fluxes, both at the surface and at the top of the atmosphere (TOA) show a negative anomaly over northern Europe (Figures 11c and 11d), induced by a decrease in both high and low cloud amounts (Figures 11e and 11f). They show also a positive anomaly in west North Africa, certainly attributable to a combination of high cloud amount and a high atmospheric concentration of dust over this region (Figure 6c).

[40] The radiative fluxes do not exceed anomalies from −8 to 4 W m^{-2} (Figure 11), whereas sensible and latent heat fluxes are strongly modified over the Atlantic in our AER-ZO experiment (Figures 11g and 11h), with values from −10 to +10 W m^{-2}. We have to keep in mind that we used the same sea surface temperature forcing in all our experiments. Turbulent flux differences originate, therefore, only from thermodynamic processes on the atmosphere. Turbulent fluxes tend to strongly warm the atmosphere in southwest Greenland and to cool it on the northern coast of Europe (note that positive fluxes are oriented downward). In an idealized atmosphere, where the potential vorticity is uniform, a warm (cold) surface anomaly is associated with a cyclonic (anticyclonic) anomaly in the midtroposphere downstream of the surface anomaly. This type of atmospheric response corresponds to a transient response to a surface anomaly. These baroclinic transient responses can interact with the barotropic structure of the weather regimes. In our simulation, the surface variations of the heat fluxes should destabilize the NAO– regime, characterized by a high-pressure system over Greenland and low pressures over Europe and the tropical Atlantic (Figure 1). This might be an explanation for the 1.78 day decrease in the NAO– regime persistence modeled on the AER-ZO experiment.

[41] As we said previously, the atmospheric energy balance is quite difficult to link with aerosol distributions, because of all the interactions that occur in the climate system and, in particular, through cloud feedbacks. Considering shortwave fluxes, the signature of sulfate is not pointed out between the AER-ZO and CTL experiments, whereas this aerosol is known to strongly scatter solar radiation. The same conclusion is drawn for absorbing BC.

[42] In addition, we have to keep in mind that our sensitivity experiments did not take into account the variations of sea-salt and OC aerosols associated with each weather regime. These aerosols are known to have a strong impact on the atmosphere energy balance, being a nonnegligible component of the total AOT [*Kinne et al.*, 2006]. Some significant variations of radiative fluxes could be modeled in a simulation capable of taking into account the burden variations of these aerosols.

[43] Moreover, additional simulations conducted with online diagnostics of aerosol forcing in the ARPEGE-Climat model could help us understand more accurately the impact of the aerosol distribution associated with the zonal regime on the NAO– persistence. A similar analysis could be performed to explain the decrease in the zonal regime persistence in a winter simulation forced by the aerosol distribution associated with the blocking regime.

5. Conclusion

[44] This study focuses on the interactions between aerosol atmospheric concentration and winter weather regimes in the NAE region (20°N–80°N, 80°W–40°E). It is divided into two parts. In the first part, the Chemical-Transport Model MOCAGE is used to perform a simulation from 2000 to 2005, using the meteorological data of the ECMWF IFS model. The aerosol burden anomalies induced by each weather regime are assessed, the anomalies of aerosol sinks and sources are analyzed, and the modifications of the aerosol transport involved by wind anomalies are evaluated. Atmospheric dynamical processes associated with the different weather regimes can impact by up to 25% the burden of sulfate and BC and by up to 80% the burden of dust. As a consequence, AOT can be modified by up to 30% over the NAE region. These AOT variations are therefore attributable only to BC, dust, and sulfate burden variations, whereas OC and sea salt are not described in the CTM that we used. However, these AOT variations may have an impact on the weather in the NAE region. In the second part, the patterns of aerosol anomalies associated

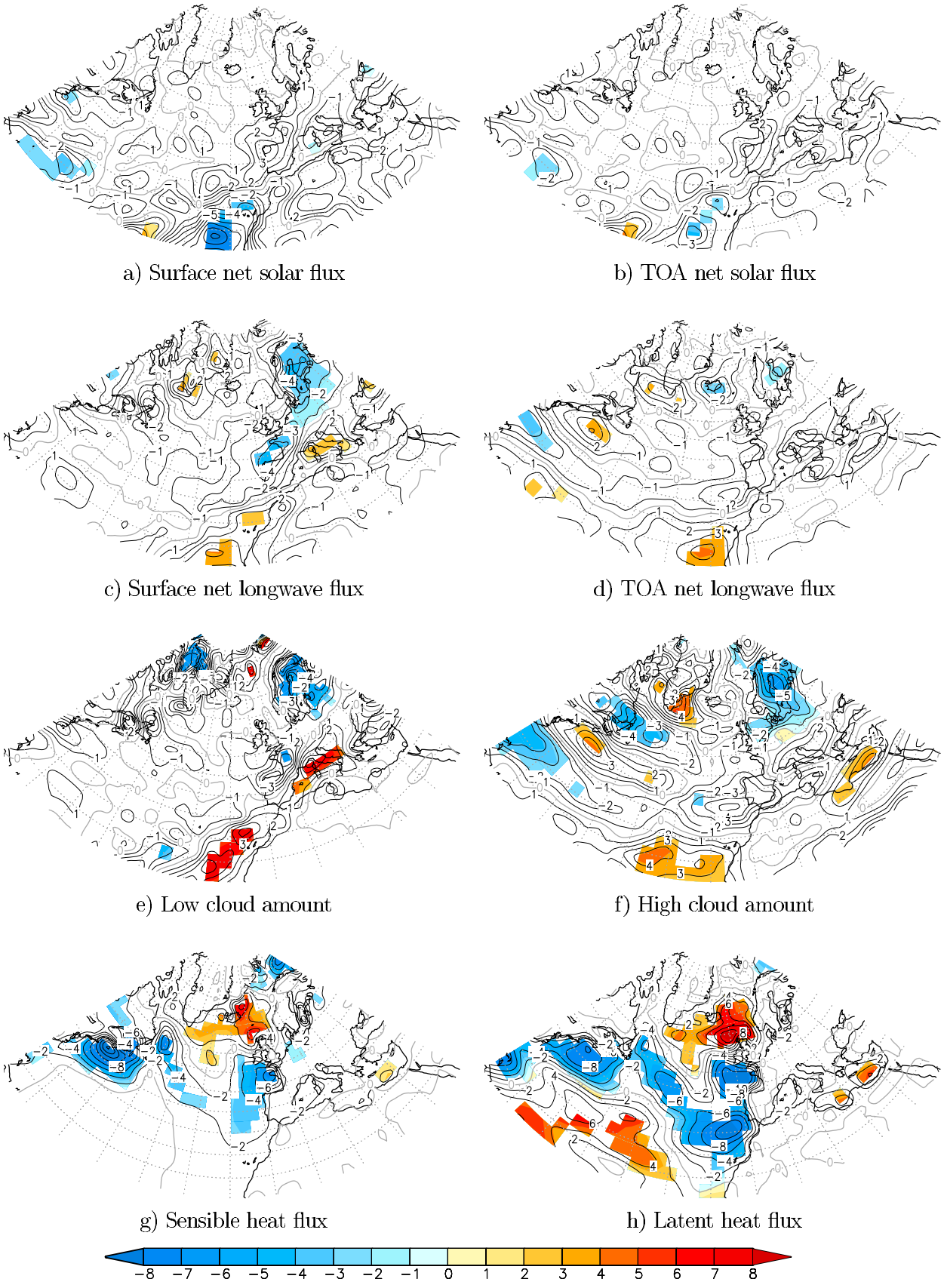

Figure 11. Differences in heat fluxes (in W m^{-2}) and low and high cloud amounts (in percentage) (AER-ZO − CTL) during the NAO– regime (see text for description). Positive fluxes are directed downward.

with each weather regime are used to force experiments performed with the ARPEGE-Climat model. These experiments are used to discuss the role of the aerosol concentration in the atmosphere on the persistence of a specified weather regime or on transition toward another weather regime during the winter. When the simulation is forced with the pattern of aerosol associated with a weather regime, neither the occurrence nor the persistence of this weather regime is modified by aerosols. This suggests that aerosols do not have a direct impact on weather regime characteristics. However, the mean persistence of the NAO– and the zonal regime are reduced by 1.78 and 0.88 days, respectively, when the atmosphere is forced with the patterns of aerosol induced by the zonal regime and the blocking regime, respectively. This suggests that the interaction with the atmospheric aerosol concentration could destabilize the NAO– regime that occurs after a zonal episode. The same conclusion can be exposed for a zonal regime that occurs after a blocking episode. In the future, these interesting aspects could help to a better prevision of weather regimes in the NAE region.

[45] The destabilization of the NAO– regime attributable to an aerosol forcing corresponding to the zonal regime is linked to modifications in the atmospheric energy budget in our simulation. The aerosol radiative forcing associated with all the climate retroactions, particularly with cloud feedback, induces strong modifications of turbulent fluxes over the Atlantic Ocean, which destabilize the high-pressure system over Greenland characteristic of the NAO– phase. Additional simulations, using an AGCM with diagnostics of the aerosol radiative forcing, could help distinguish this forcing from all the climate retroactions and assess more accurately the impact of the aerosol distributions associated with each weather regime.

[46] **Acknowledgments.** This work formed part of a Ph.D. thesis at the Centre National de Recherches Météorologiques (CNRM-GAME), Toulouse, funded by Météo-France and the CNRS. We thank Soline Bielli for her help in applying the weather regime classification and Pascal Terray and Eric Maisonnave for the availability of their statistical package STATPACK. The figures have been prepared using GrADS free software.

References

Albrecht, B. A. (1989), Aerosols, cloud microphysics and fractional cloudiness, *Science*, *245*, 1227–1230, doi:10.1126/science.245.4923.1227.

Ångström, A. (1962), Atmospheric turbidity, global illumination and planetary albedo of the earth, *Tellus*, *14*, 435–450.

Bechtold, P., E. Bazile, F. Guichard, P. Mascart, and E. Richard (2001), A mass flux convection scheme for regional and global models, *Q. J. R. Meteorol. Soc.*, *127*, 869–886, doi:10.1002/qj.49712757309.

Boucher, O., and U. Lohmann (1995), The sulfate-CCN-cloud albedo effect, a sensitivity study using two general circulation models, *Tellus, Ser. B*, *47*, 281–300.

Cassou, C. (2008), Intraseasonal interaction between the Madden-Julian Oscillation and the North Atlantic Oscillation, *Nature*, *455*, 523–527, doi:10.1038/nature07286.

Cassou, C., C. Deser, L. Terray, J. W. Hurrell, and M. Drevillon (2004), Summer sea surface temperature conditions in the North Atlantic and their impact upon the atmospheric circulation in early winter, *J. Clim.*, *17*, 3349–3363, doi:10.1175/1520-0442(2004)017<3349:SSSTCI>2.0.CO;2.

Dandin, P., and J. J. Morcrette (1996), The ECMWF FMR scheme in the Météo-France climate model Arpege-climat, *Note 50*, pp. 74, CNRM, Météo-France, Toulouse, France.

Dentener, F., et al. (2006), Emissions of primary aerosol and precursor gases in the years 2000 and 1750 prescribed data-sets for AeroCom, *Atmos. Chem. Phys.*, *6*, 4321–4344.

Déqué, M., et al. (1999), ARPEGE version 3, documentation algorithmique et mode d'emploi (in French), CNRM/GMGEC, Toulouse, France.

Douville, H., J.-F. Royer, and J.-F. Mahfouf (1995a), A new snow parameterization for the Météo-France climate model. Part I: Validation in stand-alone experiments, *Clim. Dyn.*, *12*, 21–35, doi:10.1007/BF00208760.

Douville, H., J.-F. Royer, and J.-F. Mahfouf (1995b), A new snow parameterization for the Météo-France climate model. Part II: Validation in a 3-D GCM experiments, *Clim. Dyn.*, *12*, 37–52, doi:10.1007/BF00208761.

Fouquart, Y., and B. Bonnel (1980), Computations of solar heating of the earth's atmosphere: A new parameterization, *Beitr. Phys. Atmos.*, *53*, 35–62.

Gibelin, A. L., and M. Déqué (2003), Anthropogenic climate change over the Mediterranean region simulated by a global variable resolution model, *Clim. Dyn.*, *20*, 327–339.

Gibson, J. K., P. Kallberg, S. Uppala, A. Hernandez, A. Nomura, and E. Serrano (1997), ERA description, *ECMWF Reanalysis Proj. Rep. Ser. 1*, p. 66, Eur. Cent. for Medium-range Weather Forecasts, Reading, U. K.

Heintzenberg, J., and R. J. Charlson (2009), *Clouds in the Perturbed Climate System, Their Relationship to Energy Balance, Atmospheric Dynamics, and Precipitation*, MIT Press, Cambridge, MA, 576 pp.

Hjellbrekke, A.-G. (2004), Data report 2002, acidifying and eutrophying compounds, Tech. Rep. EMEP/CCC Rep. 1/2004, EMEP, Oslo, Norway.

Hohenegger, C., and P. L. Vidale (2005), Sensitivity of the European climate to aerosol forcing as simulated with a regional climate model, *J. Geophys. Res.*, *110*, D06201, doi:10.1029/2004JD005335.

Intergovernmental Panel on Climate Change (2007), *Climate Change 2007: The Scientific Basis*, Cambridge Univ. Press, Cambridge, U.K.

Josse, B., P. Simon, and V.-H. Peuch (2004), Radon global simulations with the multiscale chemistry and transport model MOCAGE, *Tellus, Ser. B*, *56*, 339–356.

Kasper-Giebl, A. (2000), Scavenging efficiency of "aerosols carbon" and sulphate in supercooled clouds at MT Soonblick (3106 m a.s.l., Austria), *J. Atmos. Chem.*, *35*, 33–46, doi:10.1023/A:1006250508562.

Kinne, S., et al. (2006), An AeroCom initial assessment—optical properties in aerosol component modules of global models, *Atmos. Chem. Phys.*, *6*, 1815–1834.

Kirkevag, A., T. Iversen, Ø. Seland, J. B. Debernard, T. Storelvmo, and J. E. Kristjansson (2008), Aerosol-cloud-climate interactions in the climate model CAM-Oslo, *Tellus, Ser. A*, *60*, 492–512, doi:10.1111/j.1600-0870.2008.00313.x.

Koch, D. (2001), Transport and direct radiative forcing of carbonaceous and sulfate aerosols in the GISS GCM, *J. Geophys. Res.*, *106*(D17), 20,311–20,332, doi:10.1029/2001JD900038.

Langner, J., and H. Rodhe (1991), A global three-dimensional model of the tropospheric sulphur cycle, *J. Atmos. Chem.*, *13*, 225–263, doi:10.1007/BF00058134.

Lohmann, U., and J. Feichter (2005), Global indirect effects: A review, *Atmos. Chem. Phys.*, *5*, 715–737.

Louis, J.-F. (1979), A parametric model of vertical eddy fluxes in the atmosphere, *Boundary Layer Meteorol.*, *17*, 187–202, doi:10.1007/BF00117978.

Mahfouf, J. F., A. Manzi, J. Noilhan, H. Giordani, and M. Déqué (1995), The land surface scheme ISBA within the Météo-France climate model ARPEGE. Part I. Implementation and preliminary results, *J. Clim.*, *8*, 2039–2057, doi:10.1175/1520-0442(1995)008<2039:TLSSIW>2.0.CO;2.

Marmer, E., B. Langmann, K. Hungershöfer, and T. Trautmann (2007), Aerosol modeling over Europe: 2. Interannual variability of aerosol shortwave direct radiative forcing, *J. Geophys. Res.*, *112*, D23S16, doi:10.1029/2006JD008040.

Martet, M., V.-H. Peuch, B. Laurent, B. Marticorena, and G. Marticorena (2009), Evaluation of long-range transport and deposition of desert dust with the CTM MOCAGE, *Tellus, Ser. B*, *61*, 449–463.

Masson, V., J. L. Champeaux, F. Chauvin, C. Meriguet, and R. Lacaze (2003), A global database of land surface parameters at 1 km resolution in meteorological and climate models, *J. Clim.*, *16*, 1261–1282.

McCormick, R. A., and J. H. Ludwig (1967), Climate modifications by atmospheric aerosols, *Science*, *156*, 1358–1359, doi:10.1126/science.156.3780.1358.

Ménégoz, M., D. Salas y Melia, M. Legrand, H. Teyssèdre, M. Michou, V.-H. Peuch, M. Martet, B. Josse, and I. Dombrowski-Etchevers (2009), Equilibrium of sinks and sources of sulphate over Europe: Comparison between a six-year simulation and EMEP observations, *Atmos. Chem. Phys.*, *9*, 4505–4519.

Michelangeli, P. A., R. Vautard, and B. Legras (1995), Weather regimes: Recurrence and quasi stationarity, *J. Atmos. Sci.*, *52*, 1237–1256, doi:10.1175/1520-0469(1995)052<1237:WRRAQS>2.0.CO;2.

Michou, M., and V.-H. Peuch (2002), Surface exchanges in the MOCAGE multiscale chemistry and transport model, *J. Water Sci.*, *15*, 173–203.

Nho-Kim, E.-Y., A. Peuch, M. Plu, and V.-H. Peuch (2003), *Development of the MOCAGE Atmospheric Chemistry and Transport Model*, *ADEME Rep. 9962018*, 102 pp., CNRM-GAME Météo-France, Toulouse, France.

Nho-Kim, E.-Y., M. Michou, and V.-H. Peuch (2004), Parameterization of size-dependent particle dry deposition velocities for global modeling, *Atmos. Environ.*, *38*19331942 doi:10.1016/j.atmosenv.2004.01.002.

Pham, M., J.-F. Muller, G. Brasseur, C. Granier, and G. Megie (1995), A three-dimensional study of the tropospheric sulphur cycle, *J. Geophys. Res.*, *100*, 26,061–26,092, doi:10.1029/95JD02095.

Pitari, G., E. Mancini, V. Rizi, and D. T. Shindell (2002), Impact of future climate and emission changes on stratospheric aerosols and ozone, *J. Atmos. Sci.*, *59*, 414–440, doi:10.1175/1520-0469(2002)059<0414:IOFCAE>2.0.CO;2.

Reddy, M. S., O. Boucher, N. Bellouin, M. Schulz, Y. Balkanski, J.-L. Dufresne, and M. Pham (2005), Estimates of global multicomponent aerosol optical depth and direct radiative perturbation in the Laboratoire de Météorologie Dynamique general circulation model, *J. Geophys. Res.*, *110*, D10S16, doi:10.1029/2004JD004757.

Remer, L. A., et al. (2008), Global aerosol climatology from the MODIS satellite sensors, *J. Geophys. Res.*, *113*, D14S07, doi:10.1029/2007JD009661.

Reynolds, R. W., N. A. Rayner, T. M. Smith, D. C. Stokes, and W. Wang (2002), An improved in situ and satellite SST analysis for climate, *J. Clim.*, *15*, 1609–1625, doi:10.1175/1520-0442(2002)015<1609:AIISAS>2.0.CO;2.

Rongming, H., S. Planton, M. Déqué, P. Marquet, and A. Braun (2001), Why is the climate forcing of sulfate aerosols so uncertain? *Adv. Atmos. Sci.*, *18*(6), 1103–1120, doi:10.1007/s00376-001-0026-0.

Sanchez-Gomez, E., and L. Terray (2005), Large-scale atmospheric dynamics and local intense precipitation episodes, *Geophys. Res. Lett.*, *32*, L24711, doi:10.1029/2005GL023990.

Schulz, M., et al. (2006), Radiative forcing by aerosols as derived from the AeroCom present-day and pre-industrial simulations, *Atmos. Chem. Phys.*, *6*, 5225–5246.

Seinfeld, J. H., and S. N. Pandis (2006), *Atmospheric Chemistry and Physics: From Air Pollution to Climate Change*, 2nd ed., 1203 pp., John Wiley, New York.

Tanré, D., J. F. Geleyn, and J. Slingo (1984), First results of the introduction of an advanced aerosol-radiation interaction in the ECMWF low resolution global model, in *Aerosols and Their Climatic Effects*, edited by H. E. Gerber and A. Deepak, pp. 133–177, A. Deepak, Hampton, Va.

Tegen, I., P. Hollrig, M. Chin, I. Fung, D. Jacob, and J. Penner (1997), Contribution of different aerosol species to the global aerosol extinction optical thickness: Estimates from model results, *J. Geophys. Res.*, *102*, 23,895–23,915, doi:10.1029/97JD01864.

Textor, C., et al. (2006), Analysis and quantification of the diversities of aerosol life cycles within AeroCom, *Atmos. Chem. Phys.*, *6*, 1777–1813.

Teyssèdre, H., et al. (2007), A new tropospheric and stratospheric Chemistry and Transport Model MOCAGE-Climat for multi-year studies: Evaluation of the present-day climatology and sensitivity to surface processes, *Atmos. Chem. Phys.*, *7*, 58155860.

Turco, R. P., R. C. Whitten, O. B. Toon, J. B. Pollack, and P. Hamill (1980), Stratospheric aerosols and climate, *Nature*, *283*, 283–286, doi:10.1038/283283a0.

Twomey, S. (1977), The influence of pollution on the short wave albedo of clouds, *J. Atmos. Sci.*, *34*, 1149–1152, doi:10.1175/1520-0469(1977)034<1149:TIOPOT>2.0.CO;2.

Uppala, S., P. Kallberg, A. Hernandez, S. Saarinen, M. Fiorino, X. Li, K. Onogi, N. Sokka, U. Andrae, and V. da Costa Bechtol (2004), ERA-40: ECMWF 45-year reanalysis of the global atmosphere and surface conditions 1957-2000, *ECMWF Newsl.*, *101*, 2–21.

Vautard, R. (1990), Multiple weather regimes over the North Atlantic: Analysis of precursors and successors, *Mon. Weather Rev.*, *118*, 2056–2081, doi:10.1175/1520-0493(1990)118<2056:MWROTN>2.0.CO;2.

Wesely, M. L. (1989), Parameterization of surface resistances to gaseous dry deposition in regional-scale models, *Atmos. Environ.*, *23*, 1293–1304, doi:10.1016/0004-6981(89)90153-4.

Williamson, D. L., and P. J. Rasch (1989), Two-dimensional semi-Lagrangian transport with shape preserving interpolation, *Mon. Weather Rev.*, *117*, 102–129, doi:10.1175/1520-0493(1989)117<0102:TDSLTW>2.0.CO;2.

V. Guemas, M. Ménégoz, D. Salas y Melia, and A. Voldoire, CNRM/GAME, Météo-France, 42 Avenue Gaspard Coriolis, Toulouse 31057, France. (menegozmartin@yahoo.fr)